Carranza-Torres, C. and D. Saftner (2020). Computational tools for the analysis of stability of embankments in frictional-cohesive soils. In *Proceedings of the University of Minnesota 68th Annual Geotechnical Engineering Conference*. Minneapolis, Minnesota. February 27, 2020.

Computational tools for the analysis of stability of embankments in frictional-cohesive soils

Carlos Carranza-Torres[1], Ph.D., P.E. and David Saftner[2], Ph.D., A.M.ASCE

Department of Civil Engineering, University of Minnesota, Duluth Campus, 1405 University Drive, Duluth, MN 55812; email: [1] carranza@d.umn.edu; [2] dsaftner@d.umn.edu

ABSTRACT

This paper presents a series of computational tools for quick estimation of factors of safety and critical circular failure surface location for embankments. The embankments are assumed to be made of homogeneous frictional-cohesive dry soils, obeying a linear Mohr-Coulomb shear strength criterion. Cases of a firm horizon that the failure surface cannot cut through are considered to exist at the base of the embankment or at great depth. The latter case corresponds to the case of a slope in homogeneous soil. Dimensionless functions defining the factor of safety and position of the critical failure surface are constructed using the Bishop method of slices in the commercial limit equilibrium software SLIDE. Results are implemented in a computer spreadsheet that is made available for free downloading. Formulas for quick evaluation of factors of safety are also presented. The effect of the cohesion and friction angle of the soil and the position of the firm horizon on the resulting factors of safety and depth of the failure surface are discussed. An application example solved with the proposed tools and with the shear strength reduction technique implemented in the commercial software FLAC is presented. Although the tools provided in this paper have been developed for teaching basic slope stability analysis in an undergraduate soil mechanics course, the tools could be useful when performing preliminary estimates of factors of safety of embankments in actual geotechnical design practice.

INTRODUCTION

Computation of factor of safety against failure and location of the critical failure surface are the basis of the current practice of slope stability analysis in geotechnical engineering. These stability analyses are an essential component in the design of embankments and cuts for highways, levees, dams and dikes (Terzaghi et al. 1996; Coduto et al. 2011; Das & Sobhan 2018).

Various methods exist for computing the factor of safety and location of the critical failure surface for slopes. Among them, *limit equilibrium* methods, *limit analysis* methods and *full numerical* methods (e.g., Potts & Zdravkovic 1999; Davis & Selvadurai 2005). The so-called *shear strength reduction technique*, normally implemented in finite element or finite difference software (both tools being examples of implementation of the full numerical methods mentioned above), is another method for computing the stability of a slope that has gained popularity in the last two decades (e.g., Dawnson et al. 1999; Griffiths & Lane 1999; Hammah et al. 2007). All existing analysis methods, with a few exemptions (e.g., analytical models that consider a planar failure surface), require use of computer software for their implementation, as they are computational-intensive. In this sense, it is remarkable that in contrast with other problems in geotechnical engineering, there

are no rigorous analytical (closed-form) solutions available for computing the factor of safety and position of the critical failure surface for embankments or slopes. Therefore, with the lack of a *true* exact solution for the problem to be taken as a benchmark, the methods used in stability analyses of embankments or slopes (i.e., limit equilibrium methods, limit analysis methods and full numerical methods), are interpreted to give *approximate* solutions to the problem only.

Despite of its introduction in the middle of the last century, the *method of slices*, which is a particular formulation of the *limit equilibrium* method, is still the most popular method to estimate the factor of safety and location of the critical failure surface for slopes (e.g., Abramson et al. 2002; Duncan et al. 2014). Within the method of slices, there exist various formulations, including the Bishop (1955), Janbu (1954a, 1954b), Spencer (1967) and Morgenstern-Price (1965) methods. The Bishop method is popular since it gives similar results (i.e., factors of safety and location of the failure surface) as those obtained with more elaborated limit equilibrium methods (e.g., the Spencer and the Morgenstern-Price methods), with less computing effort (Abramson et al. 2002). Implementation of the Bishop method of slices to compute factor of safety and location of the critical circular failure surface for a slope requires use of specialized computer software. There exist various commercial packages of this type, e.g., GEO05 (Fine Inc. 2016), SLIDE (Rocscience Inc. 2015), SLOPE/W (Geo-Slope Inc. 2012), XSTABL (Interactive Software Designs Inc. 2007), among others.

Considering that computational-intensive methods are required for the determination of factor of safety and location of critical failure surface, authors have proposed *dimensionless charts* as a means of summarizing and conveying the results of slope stability analyses (e.g., Taylor 1948; Bishop & Morgenstern 1960; Spencer 1967; O'Connor & Mitchell 1977; Michalowski 2002; Baker 2003).

Among the existing stability charts obtained from limit equilibrium models, the ones presented in the book by Hoek & Bray (1974, 1977, 1981) (also, Wyllie & Mah 2004 and Wyllie 2018) deserve particular attention. These stability charts, which apply to slopes in rock masses assumed to obey the Mohr-Coulomb shear failure criterion, use a particular form of dimensionless scaling originally proposed by Bell (1966) that allows a compact representation of factor of safety for slopes. Since then, other authors have used the scaling rule proposed by Bell (1966) to produce dimensionless charts (e.g., Cousins 1978; Michalowski 2002; Steward et al. 2010).

This paper extends the dimensionless representations presented in Hoek & Bray (1981), focusing in the problem of *soil embankment* stability, with particular regard to the existence of a *firm* horizon beneath the embankment that the failure surface cannot cut through. Two limiting cases of embankments are considered in this paper, one in which the firm horizon (or *firm foundation*) is located at the base of the embankment, and the other in which the firm foundation is located at great depth, and therefore the case becomes that of a *slope* built or cut in a soil mass.

The developments presented in this paper build on and extend the developments in a previous paper (Carranza-Torres & Hormazabal 2018) which re-evaluated and extended the dimensionless representations originally proposed by Hoek & Bray (1981) for the general case of slopes in rock masses, without consideration of the existence of a tension crack. Based on Carranza-Torres & Hormazabal (2018), this paper provides algebraic equations obtained from regression analysis of factors of safety for embankments obtained with limit equilibrium models. It also provides a computer EXCEL workbook (Microsoft 2016) that can be conveniently used to determine factors

of safety and position of the critical (assumed circular) failure surfaces for the two limiting cases of embankments mentioned above.

PROBLEM STATEMENT

The problem considered in this paper is shown in Figure 1. An embankment is built of an assumed homogeneous, isotropic and dry soil of unit weight γ, that obeys the Mohr-Coulomb shear failure criterion, and that is characterized by a cohesion c, an internal friction angle ϕ, and null tensile strength. On the plane of analysis, the embankment is wide enough so that determining the stability of the embankment involves analyzing the stability of one of the faces only. According to Figure 1, the face is assumed to have an inclination angle α and height H. A system of cartesian coordinates (x, y) is assumed to have its origin at the *toe* of the embankment (point O in Figure 1).

Two cases are considered with regard to the position of a horizontal *firm foundation*. The first case corresponds to the firm foundation located at the *embankment base*, as represented in Figure 1. The second case corresponds to the firm foundation located at *great depth*, with the case now corresponding to that of a slope built or excavated in homogeneous soil.

When the shear strength of the soil is affected by a scalar factor of safety, the embankment in Figure 1 is assumed to be in a limit state of equilibrium with a critical *circular* failure surface of radius R and center of coordinates x_c and y_c. Because the firm foundation represented in Figure 1 prevents the failure surface from extending beyond the embankment base, the surface is comprised of the arcs $A-A'$ and $C'-B'$, and the linear segments $A'-C'$ and $B'-B$ (the latter associated with the development of a tension crack). Therefore, for a firm foundation at the embankment base, the failure surface follows the path $A-A'-C'-B'-B$, with the coordinates of the points being (x_A, y_A), ($x_{A'}$, $y_{A'}$), ($x_{C'}$, $y_{C'}$), etc. This critical failure surface is referred to as the critical *secant* failure surface in the legend of Figure 1.

In Figure 1, part of another critical circular failure surface referred to as critical *tangent* failure surface is represented with a discontinuous outline. This is the tangent failure surface that has been traditionally considered in the literature (Taylor 1948; Bishop & Morgenstern 1960; Morgenstern 1963; Michalowski 2002). Steward et al. (2010) showed that a *secant* critical failure surface yields a lower factor of safety compared with a *tangent* one. Based on Steward et al. (2010) and on full numerical models presented in the 'Application Example' section, the critical failure surface considered for the case of embankments in this paper is the one that follows the path $A-A'-C'-B'-B$. Figure 1 also indicates with discontinuous outline, a deeper failure surface that corresponds to the case in which the firm foundation is at great depth. This is the same critical failure surface that has been considered in Carranza-Torres & Hormazabal (2018), although without the inclusion of a tension crack.

With regard to the shape of failure surface in Figure 1, some authors have used *log-spiral* failure surfaces since such surfaces yield lower values of factor of safety compared with *circular* ones (Michalowski 2002; Michalowski 2013; Utili 2013; Utili & Abd 2016). The reason of adopting circular failure surfaces in this paper is that the commercial limit equilibrium software SLIDE, used to develop the computational tools, does not implement log-spiral failure surfaces.

According to the *method of slices*, when the *embankment* or *slope* is at a limit state of equilibrium, the soil shear strength is fully mobilized on the failure surface (Coduto et al. 2011;

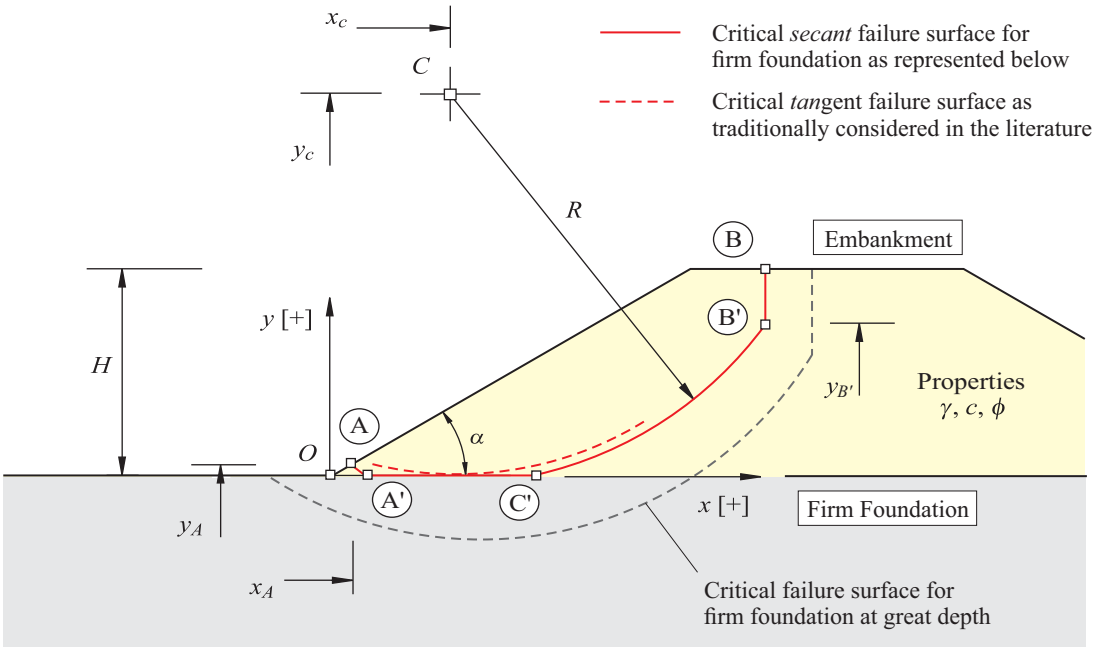

Figure 1. Problem of determining the factor of safety and position of the critical failure surface for the face of an *embankment* or *slope* in cohesive-frictional soil. A firm foundation that the failure surface cannot cut through is considered to be either at the base of the embankment or at great depth. A tension crack is allowed to develop at the crest.

Verruijt 2012; Das & Sobhan 2018). For the case of the Mohr-Coulomb soil considered in this paper, the shear strength is written as follows

$$\tau_s = \sigma_n \tan\phi + c \tag{1}$$

where τ_s and σ_n are the shear and normal stresses, respectively, at the base of an arbitrary slice on the failure surface, and ϕ and c are the internal friction angle and cohesion of the soil, respectively.

With regard to equation (1), there is abundant bibliography showing that soils are characterized by a stress dependent shear failure envelope —i.e., the relationship in equation (1) is non-linear, rather than linear (e.g., Scott 1994; Terzaghi et al. 1996; Mesri & Shahien 2003). Since the computational tools presented in this paper were originally developed for teaching basic slope stability analysis in an undergraduate soil mechanics course, the authors considered more convenient to use a simpler Mohr-Coulomb linear soil model.

The *factor of safety* (*FS*) is the ratio of the shear strength of the soil on the failure surface and the shear stress required for equilibrium (e.g., Abramson et al. 2002; Duncan et al. 2014). Of the various formulations available for computing the factor of safety, the Bishop Method (as implemented in the software SLIDE) is employed in this paper. The reader is referred to the widely available literature for more details about the implementation of the standard limit equilibrium method used in this paper (e.g., Mostyn & Small 1987; Duncan 1996; Abramson et al. 2002; Duncan et al. 2014; Huang 2014).

DIMENSIONLESS REPRESENTATIONS OF STABILITY RESULTS

In this section and in the sections that follow, the case with the firm foundation located at the embankment base (Figure 1) will be simply referred to as the *embankment* case, while the case with the firm foundation located at great depth will be referred to as the *slope* case.

For both, embankment and slope cases, and following the analysis in Carranza-Torres & Hormazabal (2018), all three mechanical variables (γ, ϕ and c) and the single length-dimension variable (H) will be grouped into a single dimensionless factor (X) as follows

$$X = \frac{\gamma H \tan\phi}{c} \tag{2}$$

According to Bell (1966) (also, Hoek & Bray 1974; Cousins 1978; Michalowski 2002; Steward et al. 2010), the factor of safety divided by the tangent of the internal friction angle of the soil ($\tan\phi$) will depend on X and on the angle of the embankment or slope face (α) only, i.e.,

$$\frac{FS}{\tan\phi} = f_{FS}(X, \alpha) \tag{3}$$

In equation (3), f_{FS} represents two distinct functions, one for the embankment case and the other for the slope case, that can be *traced* by solving a series of selected embankment and slope cases for properly chosen values of the variables X and α.

Additionally, and according to Carranza-Torres & Hormazabal (2018), all ratios of variables that characterize the position of the critical circular failure surface in Figure 1, will depend on X and α only. For example, the *scaled* abscissa and ordinate of the center of the critical circular failure are defined, respectively, as follows

$$\frac{x_c}{H} = f_{x_c}(X, \alpha) \tag{4}$$

and

$$\frac{y_c}{H} = f_{y_c}(X, \alpha) \tag{5}$$

The *scaled* abscissa and ordinate of the *starting* point of the critical circular failure surface (point A in Figure 1) are defined, respectively, as follows

$$\frac{x_A}{H} = f_{x_A}(X, \alpha) \tag{6}$$

and

$$\frac{y_A}{H} = f_{y_A}(X, \alpha) \tag{7}$$

Equations similar to the equations (4) through (7) can be stated for all other points defining the critical failure surface in Figure 1 (i.e., points A', C', B', and B).

As with the case of the function f_{FS} in equation (3), the functions f_{x_c}, f_{y_c}, f_{x_A} and f_{y_A} in equations (4) through (7) (and the similar equations for the remaining points of the critical failure surface) can be reconstructed solving a series of selected embankment and slope cases for properly chosen values of the variables X and α. Then, once these functions have been defined, the ratio of

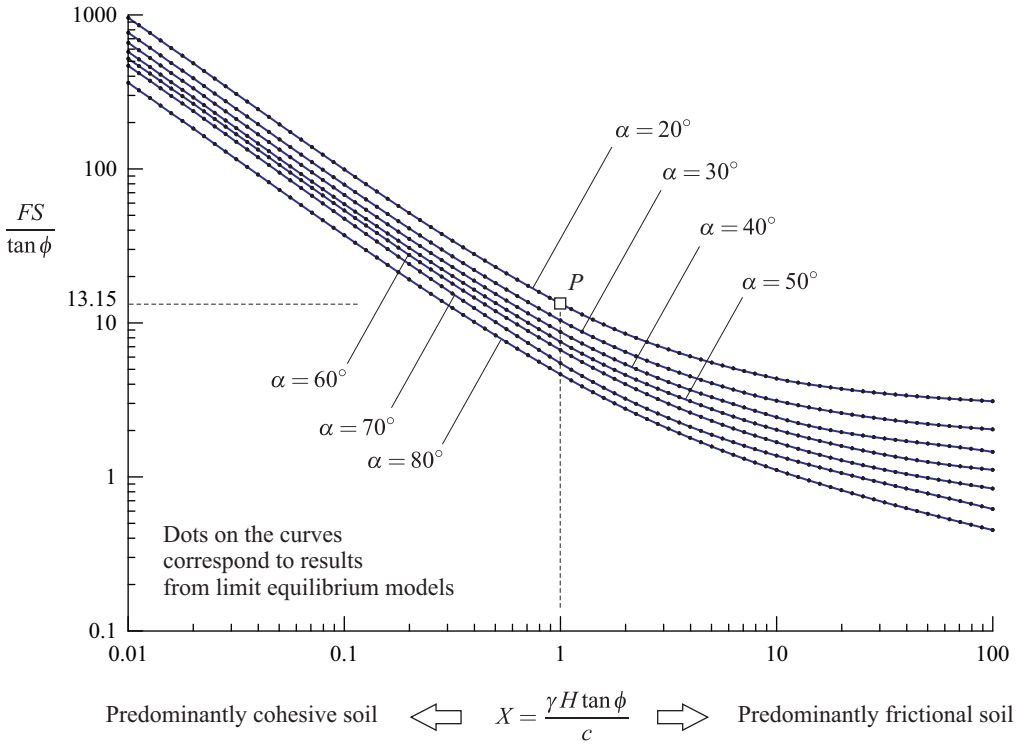

Figure 2. Dimensionless stability diagram for the estimation of scaled factor of safety for soil *embankments* with a firm foundation at the base, as represented in Figure 1.

the radius of the circular arcs forming the critical failure surface, and the height of the embankment or slope (i.e., the ratio R/H) can be computed as the distance between the points C and A in Figure 1, with the coordinates of these points expressed also as ratios of the embankment or slope height H, i.e.,

$$\frac{R}{H} = \sqrt{\left(\frac{x_c}{H} - \frac{x_A}{H}\right)^2 + \left(\frac{y_c}{H} - \frac{y_A}{H}\right)^2} \tag{8}$$

To reconstruct the functions of the dimensionless variables in equations (3) through (7), the limit equilibrium software SLIDE (Rocscience Inc. 2015) was employed. A total of 6,804 cases of embankments and slopes were evaluated using the Bishop method of slices. The input variables in the models were chosen so to obtain 81 equally spaced (in logarithm base-10 scale) embankment and slope cases with the factor X between 10^{-2} and 100. Face inclination angles between 20° and 80°, in increments of 10°, were chosen. The factors of safety and corresponding critical circular failure surfaces were determined for all cases using the 'Autorefine Search' option implemented in the software SLIDE. For the cases considering the firm foundation at the base of the embankment, the option 'Composite Surface' in the software was used. The option to create a tension crack (using default parameters) was also specified. For full details of the characteristics of the limit equilibrium models, the reader is referred to Carranza-Torres & Hormazabal (2018).

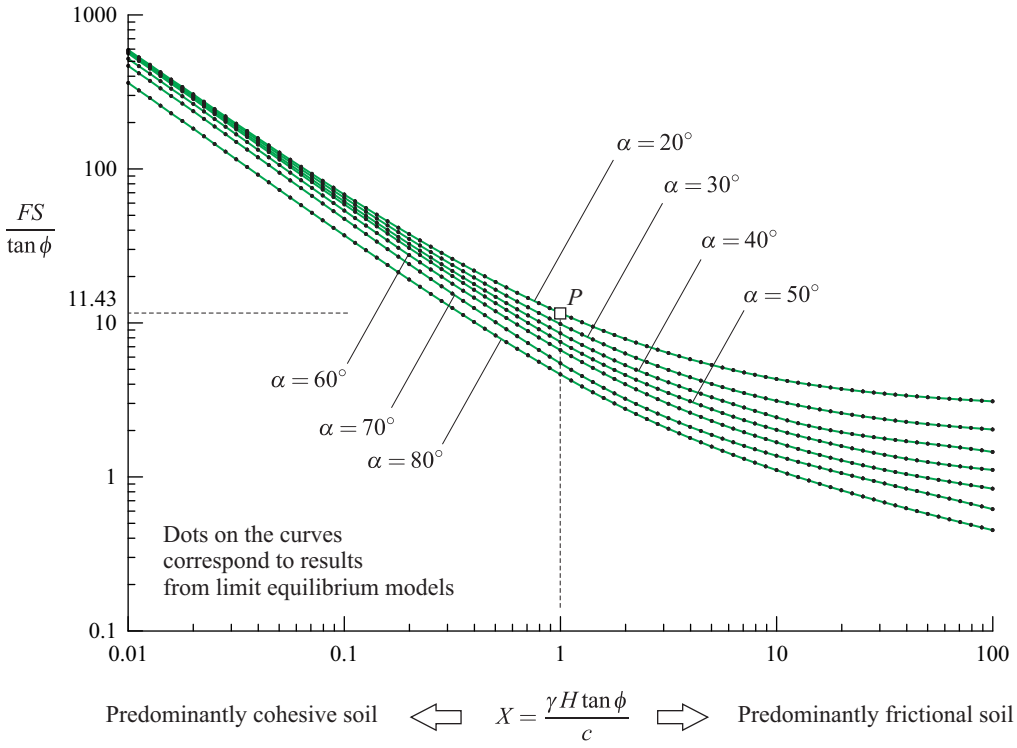

Figure 3. Dimensionless stability diagram for the estimation of scaled factor of safety for *slopes* in soils (i.e., the case in which the firm foundation in Figure 1 is at great depth).

Figure 2 shows the graphical representation of the function f_{FS} in equation (3), as obtained with SLIDE, for the *embankment* case. The diagram defines the relationship between the scaled factor of safety $FS/\tan\phi$ (vertical axis) and the ratio X (horizontal axis), for different face angles α. The small dots on the curves represent the computed limit equilibrium models. In Figure 2, as X decreases, the soil is predominantly cohesive, while as X increases, it is predominantly frictional. The figure also shows the positive influence of the cohesion of the soil on the factor of safety: for a fixed value of friction angle, the factor of safety increases with the increase in cohesion. It also shows the effect of the embankment face angle on the factor of safety: for a fixed value of the factor X, the factor of safety decreases with increase of the face angle.

Figure 3 shows the relationship between scaled factor of safety $FS/\tan\phi$ and the dimensionless variable X, for different angles α, for the *slope* case. The interpretation of Figure 3 is similar to that of Figure 2. A visual comparison of both figures indicates that the curves in Figure 3 are *shifted* downwards with respect to the curves in Figure 2, in particular, for values of face angles smaller than $\sim 50^\circ$. This implies that the factor of safety of an embankment with a firm foundation at the base will always have a factor of safety that is greater than or equal to the factor of safety of the same embankment when the firm foundation is at great depth. In other words, the stability of the embankment decreases (or remains the same, for embankments with face angles above $\sim 40^\circ$) with the increase of the depth of the firm foundation.

To quantify the difference in factors of safety for *embankments* and *slopes*, the ratio r_{SE} of the respective factors of safety is defined as follows,

$$r_{SE} = \frac{FS_{\text{slope}}}{FS_{\text{embk.}}} \tag{9}$$

Figure 4 shows the graphical representation of the ratio r_{SE} and the dimensionless variable X, for the different values of face angle α considered in Figures 2 and 3. The figure shows that the decrease in stability conditions when transitioning from *embankments* to *slopes* depends on X and α only. The lower the values of X and α, the larger the drop in factor of safety. Also, for values of X larger than ~ 1 and α larger than 50°, the factors of safety for embankments and slopes are the same. Referring to Figure 4, the discontinuity in the slope of the curve $\alpha = 40^\circ$, in the vicinity of the abscissa $X = 1$, is related to the development of the tension crack in the SLIDE models from which the curves were constructed.

To quantify the influence of the position of the firm foundation on factors of safety, the point P represented in Figures 2, 3 and 4, corresponds to *embankment* and *slope* cases for which X is 1 and α is 20°. From Figure 2, the scaled factor of safety for the *embankment* case is 13.15, whereas from Figure 3, the scaled factor of safety for the *slope* case is 11.43. From Figure 4, the decrease in the scaled factor of safety is ≈ 0.87.

For space reasons, no diagrams for the functions defining the different points that form the critical circular failure surface in Figure 1 (equations 4 through 7) are explicitly included in this paper. The diagrams can be constructed using the coordinates of the critical failure surface points that are included in the EXCEL workbook to be discussed in the section 'Computer Spreadsheet for Analysis of Stability' (the EXCEL workbook also includes coordinates of all the points represented in Figures 2 and 3).

MECHANICAL SIMILARITY OF EMBANKMENT AND SLOPE PROBLEMS

The concept of mechanical similarity of slope cases, with particular reference to mechanical similarity of scaled factors of safety and scaled position of the critical failure surface, has been introduced in Carranza-Torres & Hormazabal (2018). This section summarizes the concept, focusing on the expected decrease in stability conditions when transitioning from *embankment* cases (firm foundation at the base of the embankment) to *slope* cases (firm foundation at great depth).

Five different cases of *embankments* or *slopes*, as listed in Table 1, are considered. At first sight, and disregarding the fact that all cases have the face angle ($\alpha = 20^\circ$), these correspond to quite different embankment or slope heights, and soil properties. Nevertheless, according to the last column in Table 1, all cases are characterized by the same dimensionless variable X (equal to 1.00). Therefore, according to equations (3) through (8), the cases are expected to have the very same values of scaled factor of safety ($FS/\tan\phi$) and scaled coordinates of the different points that form the critical failure surface (i.e., the scaled coordinates of points A, A', C', etc. in Figure 1). To illustrate this, Table 2 lists the values of scaled factor of safety and scaled coordinates of the center, starting point and radius of the critical failure surface, for all cases, as obtained with equations (4) through (8) and with the EXCEL workbook to be discussed in the next section. The values listed in Table 2 result the same for all five considered cases.

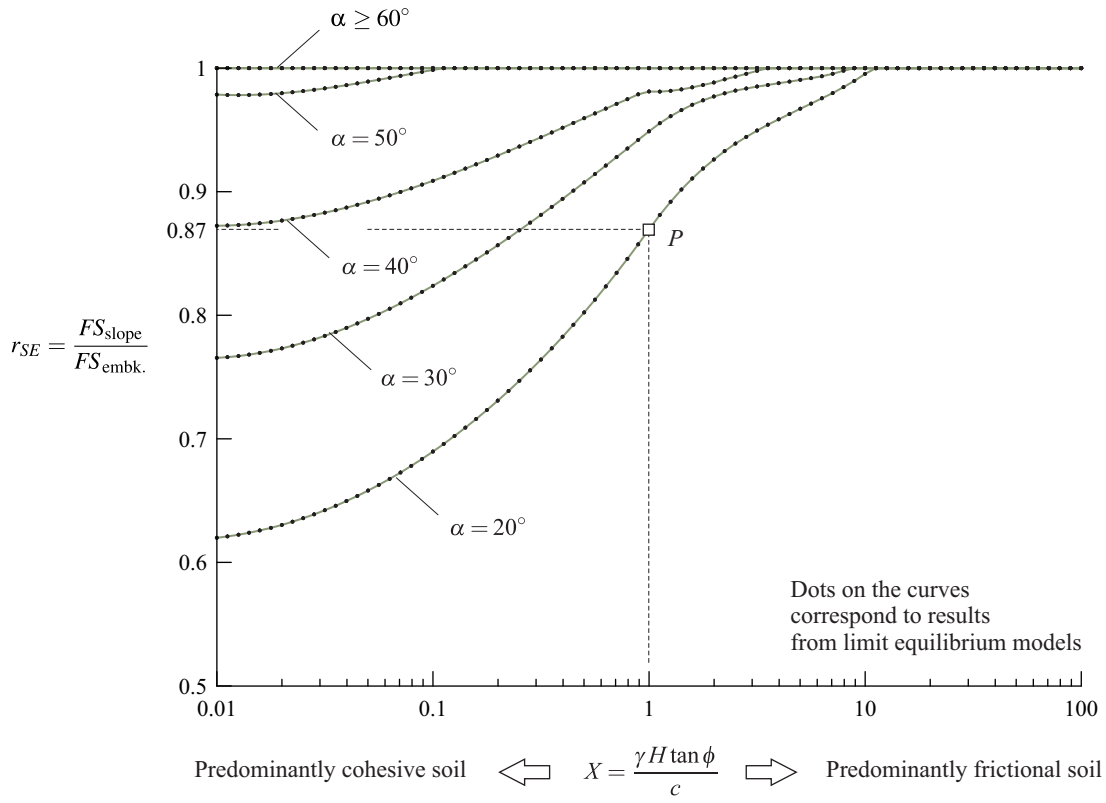

Figure 4. Ratio of factors of safety obtained with equation (9), for cases of *slopes* (firm foundation at great depth) and *embankments* (firm foundation at the embankment base).

The concept of mechanical similarity illustrated by the different cases in Tables 1 and 2, allows explanation of an observation that dates back to the early developments of computational methods for slope stability analysis in soil mechanics: *embankments and slopes in predominantly cohesive soils tend to show deeper critical failure surfaces than those in predominantly frictional soil*. Indeed, it has also been known that for slopes in purely frictional soil, the thickness of the critical failure surface becomes null, as proved by the analytical solution of an infinite slope in cohesionless soil (Scott 1994; Abramson et al. 2002; Coduto et al. 2011; Das & Sobhan 2018). It will be shown next that it is the dimensionless parameter X (equation 2) that controls how deep or shallow the critical failure surface is.

The diagrams in Figures 5a and 5b are equivalent to the diagrams already introduced in Figures 2 and 3. For clarity, only three curves corresponding to *embankment* and *slope* face angles equal to 20°, 40° and 60° are included in the diagrams. The different sketches above the curves in Figures 5a and 5b correspond to embankment and slope cases in predominantly cohesive soil (characterized by an arbitrarily chosen value $X = 0.05$), cases in a *regular* cohesive-frictional soil (arbitrarily chosen value $X = 1$), and cases in a predominantly frictional soil (arbitrarily chosen value $X = 25$). The sketches show the shape of the critical circular failure surface as obtained with the EXCEL workbook described in the next section. It is seen that when the angle of the embankment or slope face is fixed, the average thickness of the critical failure surface depends on

Table 1. Geometric characteristics and physical/mechanical soil properties for *embankments* or *slopes* that yield the same dimensionless factor X.

Case	α [°]	H [m]	γ [kN/m^3]	ϕ [°]	c [kPa]	$X = \gamma H \tan\phi \,/ c$ [-]
a	20	10.0	17.0	10.0	30.0	1.00
b		19.1	15.7	30.9	179.5	
c		20.6	16.5	5.0	29.7	
d		33.2	17.4	32.5	368.0	
e		42.4	18.1	21.1	296.1	

Table 2. Scaled factor of safety and scaled coordinates that define the position of the assumed critical failure surface, as obtained with the computational tools in this paper.

Cases	Type	$FS/\tan\phi$ [-]	x_C/H [-]	y_C/H [-]	x_A/H [-]	y_A/H [-]	R/H [-]
a, b, c, d, e	Embk.	13.15	1.17	2.60	0.25	0.09	2.67
a, b, c, d, e	Slope	11.43	1.13	2.15	-0.38	0.00	2.63

Note: For space reasons, the scaled coordinates of the remaining points defining the critical failure surface shown in Figure 1 are not listed in the table; those values result also the be the same in all five cases.

the dimensionless parameter X only. Finally, it should be noted that all five cases listed in Tables 1 and 2 plot as points B_{20} in Figures 5a and 5b. Therefore, the sketches that correspond to case B_{20} in Figures 5a and 5b are representative of the shape of the critical circular failure surface for all five cases listed in Tables 1 and 2.

COMPUTER SPREADSHEET FOR ANALYSIS OF STABILITY

Although dimensionless charts have been the traditional way of summarizing and presenting results of stability analyses, in modern geotechnical design practice, engineers typically prefer the use of computer spreadsheets over the use of these dimensionless charts (Hoek 2000).

With this idea in mind, based on Carranza-Torres & Hormazabal (2018), the results of the limit equilibrium models that allowed the functions in equations (3) through (7) to be reconstructed by discrete points, have been summarized in an EXCEL workbook (Microsoft 2016) called 'Slope Stability Calculator for Embankments in Frictional-Cohesive Soils' (Figure 6). The EXCEL workbook implements a polynomial interpolation scheme that allows the user to obtain estimates of factor of safety and location of the circular critical failure surface for any embankment or slope, provided the characteristic dimensionless factor X and the angle α fall within specified ranges.

The main interface in this EXCEL workbook is the worksheet called 'Main_Page' shown in Figure 6a. The user defines the geometry of the embankment or slope and the properties of the soil in the section entitled 'Input Data'. The results are then displayed side by side in the section 'Results', in the lower part of the same worksheet. Results are identified as Case 1, which corresponds to an embankment with the base of the firm foundation as shown in Figure 1, and Case 2, which corresponds to the firm foundation located at great depth. If the user specifies to

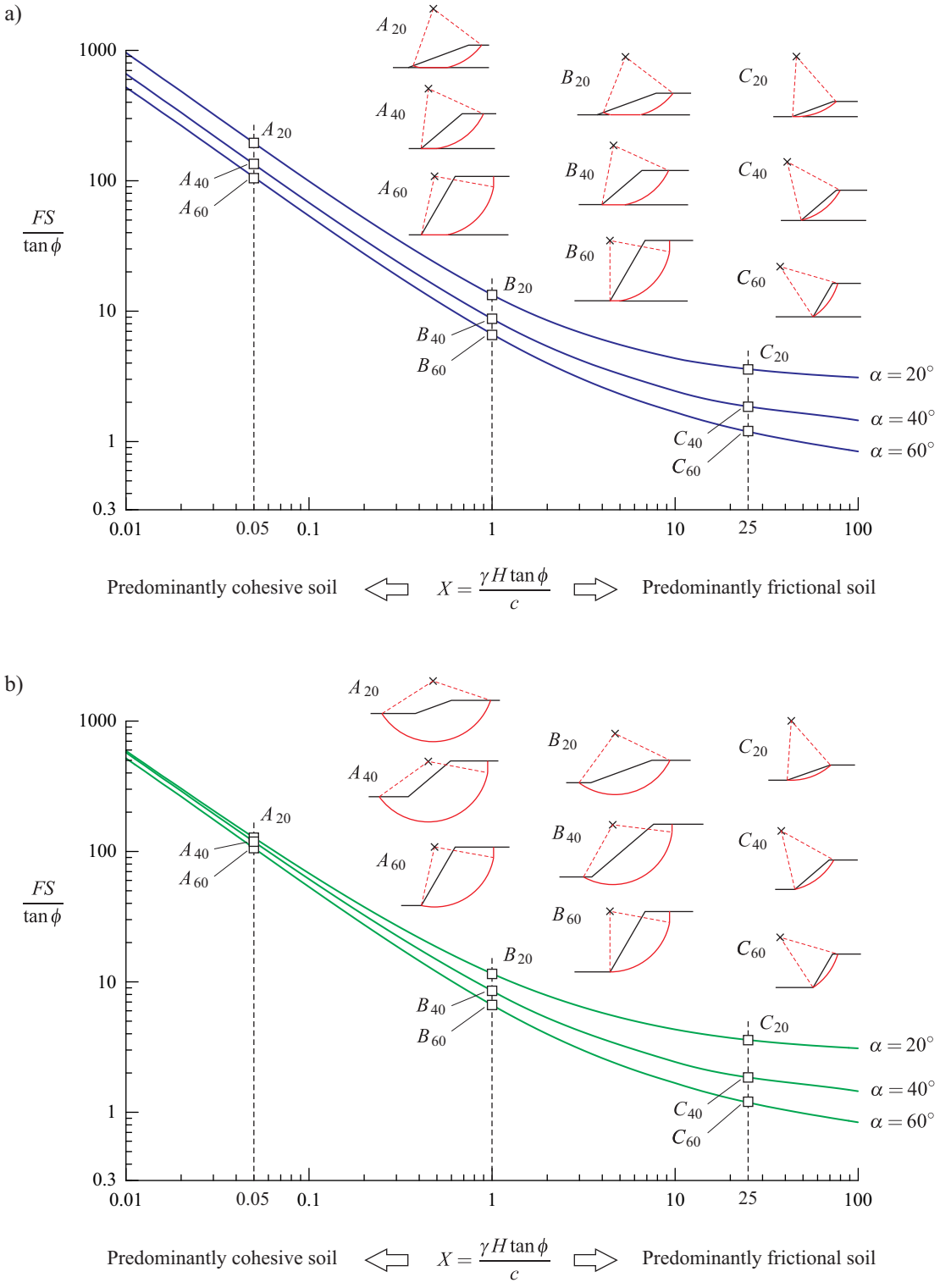

Figure 5. Dimensionless stability diagrams showing similarity of scaled factor of safety and critical failure surface location. The diagrams correspond to cases of a) *embankments*, with a firm foundation at the base; and b) *slopes*, with a firm foundation at great depth.

a)

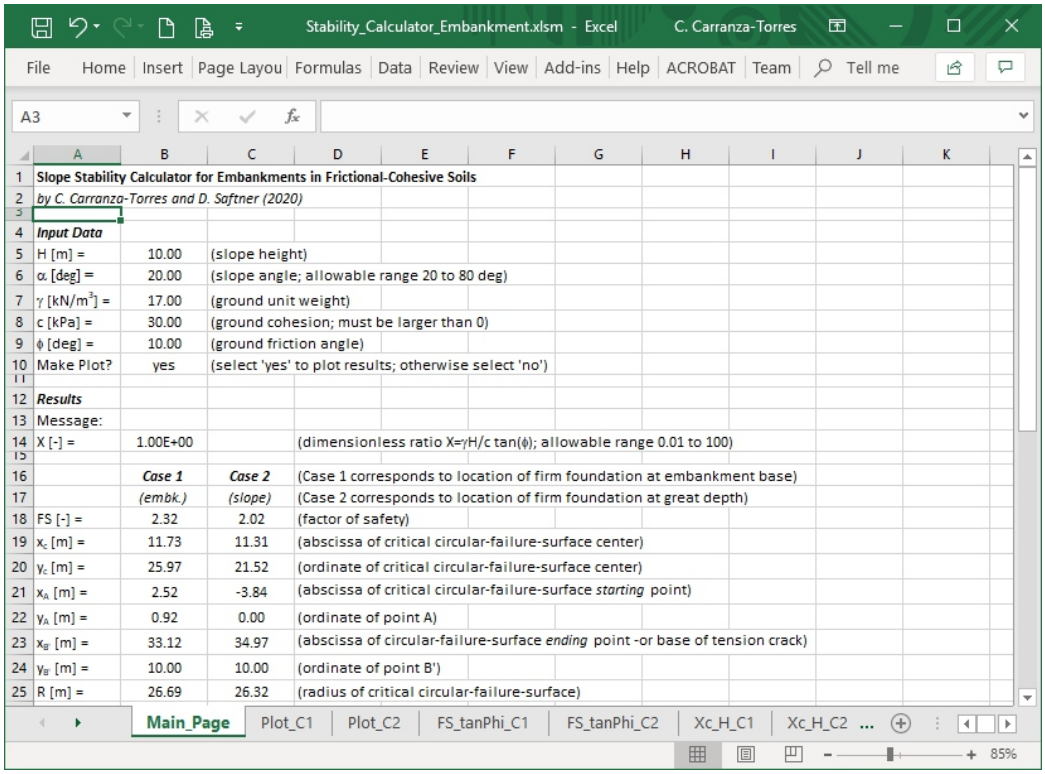

	A	B	C	D
1	**Slope Stability Calculator for Embankments in Frictional-Cohesive Soils**			
2	*by C. Carranza-Torres and D. Saftner (2020)*			
4	***Input Data***			
5	H [m] =	10.00	(slope height)	
6	α [deg] =	20.00	(slope angle; allowable range 20 to 80 deg)	
7	γ [kN/m^3] =	17.00	(ground unit weight)	
8	c [kPa] =	30.00	(ground cohesion; must be larger than 0)	
9	ϕ [deg] =	10.00	(ground friction angle)	
10	Make Plot?	yes	(select 'yes' to plot results; otherwise select 'no')	
12	***Results***			
13	Message:			
14	X [-] =	1.00E+00		(dimensionless ratio X=γH/c tan(ϕ); allowable range 0.01 to 100)
16		***Case 1***	***Case 2***	(Case 1 corresponds to location of firm foundation at embankment base)
17		*(embk.)*	*(slope)*	(Case 2 corresponds to location of firm foundation at great depth)
18	FS [-] =	2.32	2.02	(factor of safety)
19	x_c [m] =	11.73	11.31	(abscissa of critical circular-failure-surface center)
20	y_c [m] =	25.97	21.52	(ordinate of critical circular-failure-surface center)
21	x_A [m] =	2.52	-3.84	(abscissa of critical circular-failure-surface *starting* point)
22	y_A [m] =	0.92	0.00	(ordinate of point A)
23	x_B' [m] =	33.12	34.97	(abscissa of circular-failure-surface *ending* point -or base of tension crack)
24	y_B' [m] =	10.00	10.00	(ordinate of point B')
25	R [m] =	26.69	26.32	(radius of critical circular-failure-surface)

b)

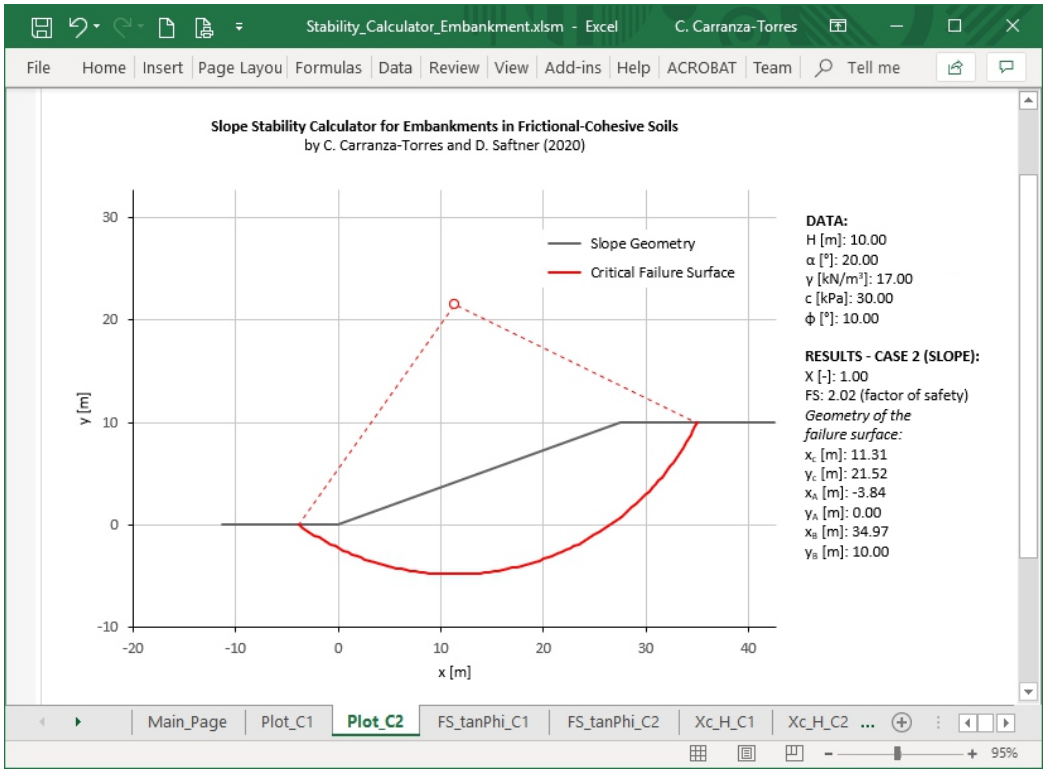

Figure 6. EXCEL workbook for implementation of stability computations. a) Main worksheet. b) Graphical representation of Case 2 (i.e., *slope* in soil).

make a plot in the input data section of the 'Main_Page' spreadsheet, two other spreadsheets in the workbook, called 'Plot_C1' and 'Plot_C2', provide a graphical representation of the embankment and slope cases (i.e., Cases 1 and 2, respectively), together with a summary of input data and results. For example, Figure 6b shows the contents of the worksheet 'Plot_C2'.

It must be emphasized that the EXCEL workbook *does not* include an implementation of the limit equilibrium method of slices to compute results of embankment problems. Instead the EXCEL workbook, simply uses *lookup* table formulas to interpolate results of models that have been *already* computed with the commercial limit equilibrium software SLIDE (Rocscience Inc. 2015), as discussed in previous sections. These results are tabulated in different worksheets, these having names which are representative of the information they contain. For example, the worksheets called 'FS_tanPhi_C1' and 'FS_tanPhi_C2' contain the resulting scaled factors of safety for different values of the dimensionless variable X and embankment or slope face angle α —i.e., the coordinates of the points in the different curves represented in Figures 2 and 3, respectively. Similarly, the worksheets called 'Xc_H_C1' and 'Xc_H_C2' contain the scaled abscissas of the center of the critical circular failure surface as a function of X and α for Cases 1 and 2, respectively, etc.

Although computation of results is implemented through table lookup formulas without the use of macros, the EXCEL workbook uses a VBA (Visual Basic for Applications) macro for constructing the plots in the worksheets 'Plot_C1' and 'Plot_C2'. Therefore, if asked by EXCEL, the user should allow the software to activate the macro in order for the plots in the worksheets 'Plot_C1' and 'Plot_C2' to be generated.

The EXCEL file corresponding to the workbook introduced above can be freely downloaded from the first author's web site, at www.d.umn.edu/∼carranza/EMBK20.

FACTOR OF SAFETY EQUATIONS FOR EMBANKMENTS AND SLOPES

Following previous developments in Carranza-Torres & Hormazabal (2018), a multiple regression analysis was carried out using the results of scaled factors of safety represented in Figures 2 and 3, for *embankments* and *slopes*, respectively. The objective of the analysis was to come up with algebraic equations to predict values of scaled factor of safety ($FS/\tan\phi$) as a function of the dimensionless factor X and the angle α, which could be used as additional tools to quickly estimate values of factors of safety.

The adjusting function was chosen to be a power inverse function of the variable X of the following form,

$$\frac{FS}{\tan\phi} = \frac{1}{\tan\alpha} + \frac{g_1(\alpha)}{X} + \frac{g_2(\alpha)}{X^{g_3(\alpha)}} \tag{10}$$

The reason for choosing an inverse function was to be able to recover the solution of an infinite slope for the case of purely frictional soil. Indeed, when X tends to infinity, all different curves in Figures 2 and 3 will become asymptotic towards the scaled factor of safety predicted by the analytical solution of an infinite slope in purely frictional soil, i.e., $FS/\tan\phi = 1/\tan\alpha$ (e.g., Scott 1994; Abramson et al. 2002; Coduto et al. 2011; Das & Sobhan 2018).

In equation (10), the functions $g_1(\alpha)$, $g_2(\alpha)$ and $g_3(\alpha)$ are cubic polynomials that are

assumed to have a discontinuity of the first and higher derivatives at $\alpha = 50^\circ$, the approximate value of slope angle above which the critical circular failure surface always start at the toe of the slope (i.e., at point 0 in Figure 1). Using standard methods of minimization of sum of square of the estimate residuals (Chapra & Canale 2015), the functions $g_1(\alpha)$, $g_2(\alpha)$ and $g_3(\alpha)$ were found to be as follows:

For the case of *embankments*,
If $\alpha \leq 50^\circ$

$$g_1(\alpha) = 5.430 - 9.180 \times 10^{-2}(\alpha - 50) - 1.904 \times 10^{-3}(\alpha - 50)^2 - 9.963 \times 10^{-5}(\alpha - 50)^3 \quad (11)$$
$$g_2(\alpha) = 1.333 + 7.563 \times 10^{-3}(\alpha - 50) + 4.674 \times 10^{-4}(\alpha - 50)^2 + 5.871 \times 10^{-6}(\alpha - 50)^3$$
$$g_3(\alpha) = 3.682 \times 10^{-1} + 3.068 \times 10^{-4}(\alpha - 50) - 3.841 \times 10^{-5}(\alpha - 50)^2 - 9.460 \times 10^{-7}(\alpha - 50)^3$$

If $\alpha \geq 50^\circ$

$$g_1(\alpha) = 5.430 - 6.067 \times 10^{-2}(\alpha - 50) + 2.088 \times 10^{-3}(\alpha - 50)^2 - 7.738 \times 10^{-5}(\alpha - 50)^3 \quad (12)$$
$$g_2(\alpha) = 1.333 + 1.721 \times 10^{-2}(\alpha - 50) - 4.454 \times 10^{-3}(\alpha - 50)^2 + 1.217 \times 10^{-4}(\alpha - 50)^3$$
$$g_3(\alpha) = 3.682 \times 10^{-1} + 7.698 \times 10^{-3}(\alpha - 50) - 1.419 \times 10^{-3}(\alpha - 50)^2 + 3.664 \times 10^{-5}(\alpha - 50)^3$$

For the case of *slopes*,
If $\alpha \leq 50^\circ$

$$g_1(\alpha) = 5.346 - 8.603 \times 10^{-3}(\alpha - 50) - 3.221 \times 10^{-4}(\alpha - 50)^2 - 1.335 \times 10^{-7}(\alpha - 50)^3 \quad (13)$$
$$g_2(\alpha) = 1.414 - 3.435 \times 10^{-2}(\alpha - 50) + 1.656 \times 10^{-3}(\alpha - 50)^2 + 2.175 \times 10^{-5}(\alpha - 50)^3$$
$$g_3(\alpha) = 3.841 \times 10^{-1} - 6.840 \times 10^{-3}(\alpha - 50) + 4.102 \times 10^{-5}(\alpha - 50)^2 + 3.573 \times 10^{-6}(\alpha - 50)^3$$

If $\alpha \geq 50^\circ$

$$g_1(\alpha) = 5.346 - 4.524 \times 10^{-2}(\alpha - 50) + 1.247 \times 10^{-3}(\alpha - 50)^2 - 6.336 \times 10^{-5}(\alpha - 50)^3 \quad (14)$$
$$g_2(\alpha) = 1.414 + 2.321 \times 10^{-3}(\alpha - 50) - 3.642 \times 10^{-3}(\alpha - 50)^2 + 1.082 \times 10^{-4}(\alpha - 50)^3$$
$$g_3(\alpha) = 3.841 \times 10^{-1} + 4.771 \times 10^{-3}(\alpha - 50) - 1.259 \times 10^{-3}(\alpha - 50)^2 + 3.398 \times 10^{-5}(\alpha - 50)^3$$

It is important to note that the regression analysis considers that the embankment or slope face angle (α) in the equations above is expressed in degrees and not in radians.

To illustrate the application of the regression equations above, Figure 7a shows a diagram that is equivalent to that in Figure 2, but constructed with equation (10), together with equations (11) and (12). At first sight, the diagrams in Figures 2 and 7a are identical. Nevertheless, because the equations used to construct the curves in Figure 7a are best fit equations obtained from regression analysis, there will be some error associated with the estimation of scaled factor of safety.

The error in the estimate of scaled factor of safety with the regression equations can be quantified using the following expression

$$\frac{FS}{\tan\phi}\ \text{Error}\ [\%] = \frac{FS/\tan\phi\ \text{(with Eq. 10)} - FS/\tan\phi\ \text{(with Eq. 3)}}{FS/\tan\phi\ \text{(with Eq. 3)}} \quad (15)$$

Equation (15) *assumes* that the factors of safety obtained with the limit equilibrium software

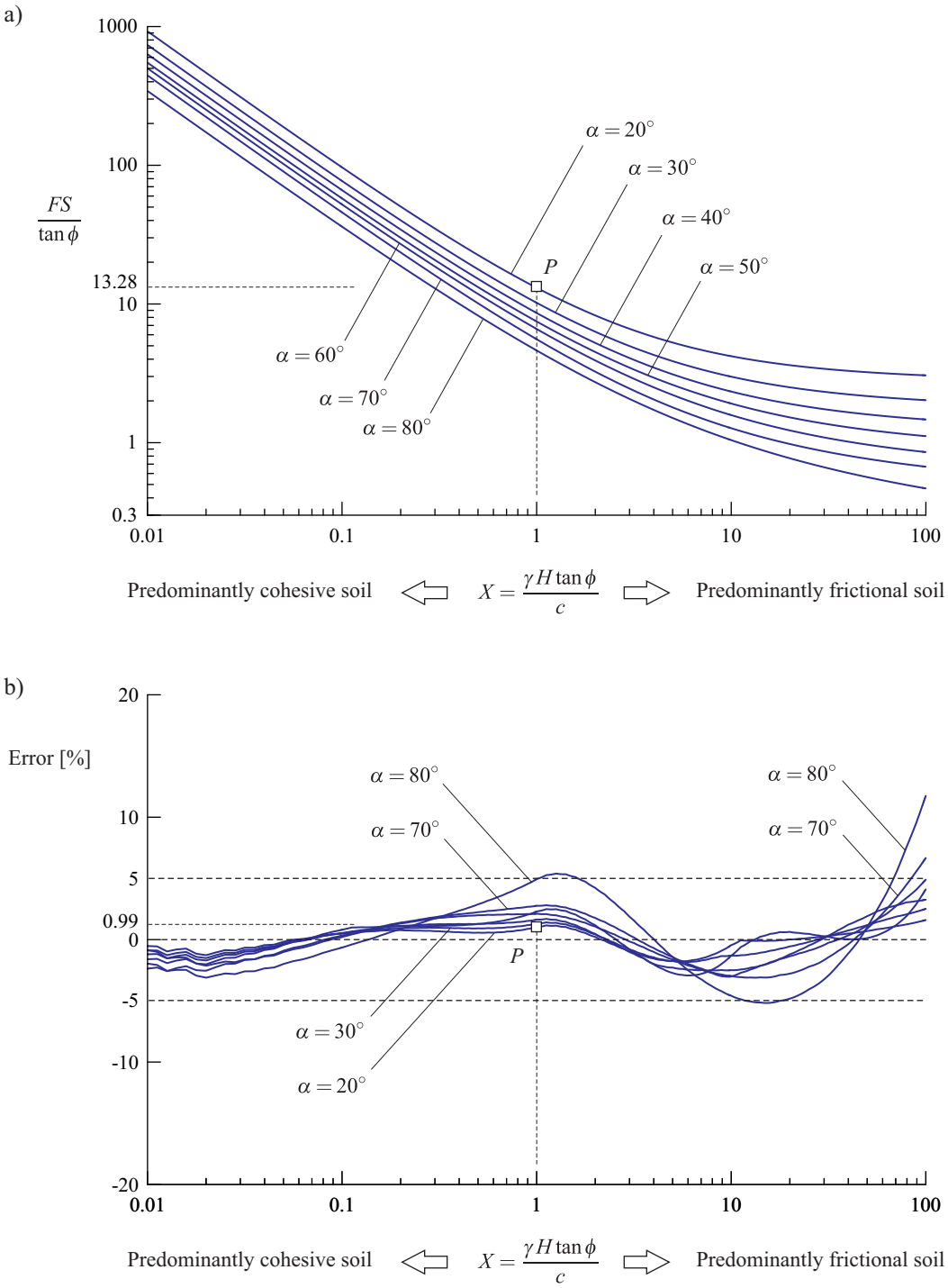

Figure 7. a) Dimensionless stability diagram for *embankments* (firm foundation at the base) equivalent to that in Figure 2, obtained with equation (10). b) Resulting error in the estimation of factor of safety with the regression formulas (equation 15).

SLIDE (equation 3) correspond to the *true* solution of the problem.

Figure 7b is the graphical representation of the error given by equation (15) for *embankments*. The figure indicates that the error associated with application of equation (10) can be positive or negative (i.e., the values of scaled factor of safety can be either overestimated or underestimated, respectively). The figure also indicates that the largest error (that in absolute value is $\sim 10\%$) occurs for the case of very steep embankment faces (angles $\alpha \geq 70^{\circ}$) and for predominantly frictional soils. Figure 7b also indicates that for embankment faces of small inclination angle, the error is not significant. For example, considering the embankment case already discussed in the section 'Dimensionless Representations of Stability Results', for which $X = 1$ and $\alpha = 20^{\circ}$, application of the regression equations (10) through (12) yields a scaled factor of safety equal to 13.28 (point *P* in Figure 7a), whereas the scaled factor of safety predicted by SLIDE is equal to 13.15 (point *P* in Figure 2). Therefore, application of the regression equations yields an error of only 0.99% (point *P* in Figure 7b).

Figures 8a and 8b show similar representations as in Figures 7a and 7b, for the case of *slopes*. Again, comparing Figures 8a and 3, it is observed that the largest error (that in absolute value is $\sim 10\%$) occurs for the case of very steep embankment or slope faces (angles $\alpha \geq 70^{\circ}$) and for the case of predominantly frictional soils. Also, for cases of relatively small embankment face inclination angle, the error is not significant (point *P* in Figure 8b).

The reason why the error becomes large for the case of embankment and slope faces with steep faces ($\geq 70\%$) in Figures 7b and 8b, is related to the inclusion of a tension crack in the limit equilibrium models used to define the dimensionless functions given by equations (3) through (7). The resulting factor of safety and location of the critical failure surface are quite sensitive to the inclusion of a tension crack in limit equilibrium models of slopes, particularly for very steep slopes with null tensile strength. The effect of the influence of the tension crack in steep slopes is put in evidence when comparing the magnitude of error for the case of *slopes* with a tension crack (Figure 8b) with the equivalent error presented in Carranza-Torres & Hormazabal (2018) for slopes without a tension crack. In the former case, the errors for slope inclination angles clearly exceed 5% in absolute value (Figure 8b), while in the latter case *all* errors are within $\pm 5\%$.

As inclusion of tension cracks in the limit equilibrium models makes the error of the regression equations increase for very steep embankments and slopes, the reader is cautioned to limit the application of the equations presented in this section to cases of embankment or slope face angles smaller than 70%.

APPLICATION EXAMPLE

This section presents an application example of stability analysis of an embankment that illustrates the use of the computational tools discussed in previous sections.

The problem involves computing the factor of safety and location of the critical circular failure surface for the face of the embankment in Figure 1 with geometry and soil properties as follows:

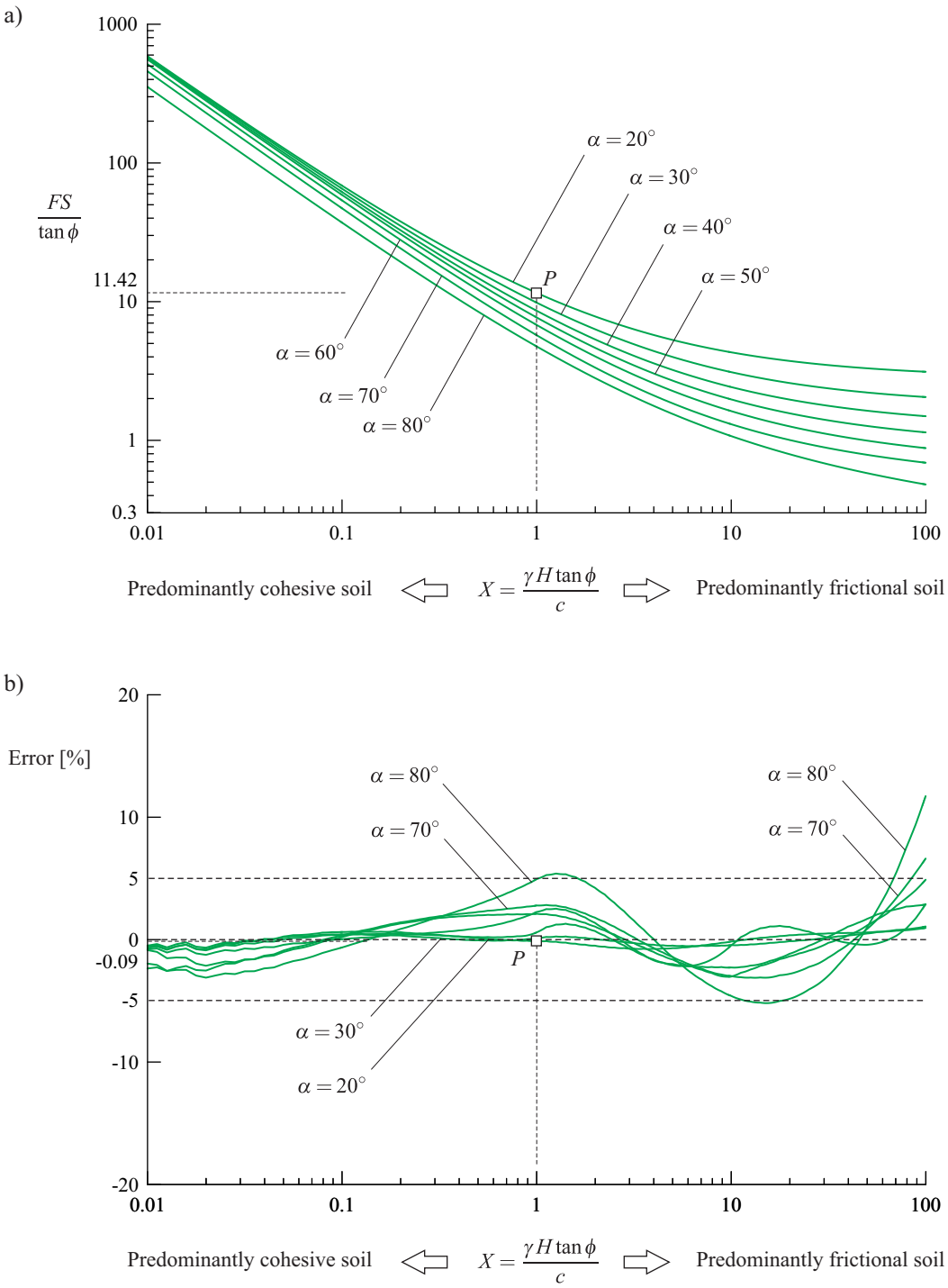

Figure 8. a) Dimensionless stability diagram for *slopes* (firm foundation at great depth) equivalent to that in Figure 3, obtained with equation (10). b) Resulting error in the estimation of factor of safety with the regression formulas (equation 15).

– Height, $H = 10$ m
– Face inclination angle, $\alpha = 20^\circ$
– Unit weight of the soil, $\gamma = 17$ kN/m^3
– Cohesion of the soil, $c = 30$ kPa
– Internal friction angle of the soil, $\phi = 10^\circ$

Cases in which the firm foundation is located at the base of the embankment, and in which the firm foundation is located at great depth will be considered separately. Following the notation of the EXCEL workbook introduced in an earlier section, the cases will be referred to as Case 1 (or *embankment* case) and Case 2 (or *slope* case), respectively.

According to the 'Dimensionless Representations of Stability Results' section, the factor of safety and location of critical failure surface depends on the dimensionless factor X, and on the face angle α (in this case, 20°). For the input values listed above, the dimensionless factor X results to be

$$X = \frac{\gamma H \tan\phi}{c} = \frac{17\,\mathrm{kN/m^3} \times 10\,\mathrm{m} \times \tan 10^\circ}{30\,\mathrm{kPa}} = 1.0 \tag{16}$$

The embankment problem introduced above corresponds to the *Case a* in the Tables 1 and 2 and to the values listed in the EXCEL workbook (Figure 6). Therefore, from Table 2 and Figure 6a, the computational tools introduced in previous sections give the following values of factor of safety and coordinates of the points that define the critical failure surface:

For Case 1 (or *embankment* case):

– Scaled factor of safety, $FS/\tan\phi = 13.15$ ($FS = 2.32$ for $\phi = 10^\circ$)
– Scaled abscissa of the center of the critical failure surface, $x_c/H = 1.17$ ($x_c = 11.7$ m for $H = 10$ m)
– Scaled ordinate of the center of the critical failure surface, $y_c/H = 2.60$ ($y_c = 26.0$ m for $H = 10$ m)
– Scaled abscissa of the *starting* point of the critical failure surface, $x_A/H = 0.25$ ($x_A = 2.5$ m for $H = 10$ m)
– Scaled ordinate of the *starting* point of the critical failure surface, $y_A/H = 0.09$ ($y_A = 0.9$ m for $H = 10$ m)
– Scaled radius of the critical failure surface, $R/H = 2.67$ ($R = 26.7$ m for $H = 10$ m)

For Case 2 (or *slope* case):

– Scaled factor of safety, $FS/\tan\phi = 11.43$ ($FS = 2.02$ for $\phi = 10^\circ$)
– Scaled abscissa of the center of the critical failure surface, $x_c/H = 1.13$ ($x_c = 11.3$ m for $H = 10$ m)
– Scaled ordinate of the center of the critical failure surface, $y_c/H = 2.15$ ($y_c = 21.5$ m for $H = 10$ m)
– Scaled abscissa of the *starting* point of the critical failure surface, $x_A/H = -0.38$ ($x_A = -3.8$ m for $H = 10$ m)

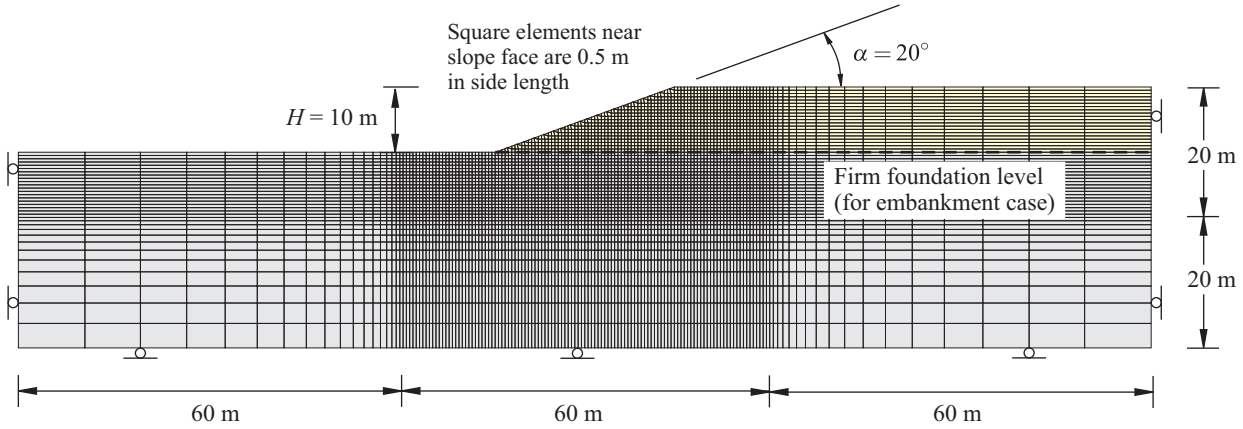

Figure 9. Geometry and mesh of elements for the embankment model solved with the finite difference software FLAC (Itasca 2016).

– Scaled ordinate of the *starting* point of the critical failure surface, $y_A/H = 0.0$ ($y_A = 0.0$ m for $H = 10$ m)
– Scaled radius of the critical failure surface, $R/H = 2.63$ ($R = 26.3$ m for $H = 10$ m)

From the resulting values of factor of safety, it is seen that Case 1 and Case 2 are *stable* (i.e., they both have a factor of safety larger than one), and according to the 'Dimensionless Representations of Stability Results' section, Case 1 has a larger factor of safety than Case 2.

The previous section illustrated the application of the regression formulas for estimating factors of safety for embankment and slope cases characterized by the particular dimensionless factor $X = 1$ and angle $\alpha = 20^\circ$ (point P in Figures 7 and 8). Those cases are the same Cases 1 and 2 considered here. Therefore, the regression analysis formulas (equations 10 through 14) give the following factors of safety:

For Case 1 (or *embankment* case):
– Scaled factor of safety, $FS/\tan\phi = 13.28$ ($FS = 2.34$ for $\phi = 10^\circ$)

For Case 2 (or *slope* case):
– Scaled factor of safety, $FS/\tan\phi = 11.42$ ($FS = 2.01$ for $\phi = 10^\circ$)

Comparing the values of factor of safety obtained with the regression formulas (equations 10 through 14) and with the EXCEL workbook, for Case 1, the formulas overestimate slightly the stability of the embankment, giving an error of 0.99% —point P in Figure 7b. For Case 2, the formulas underestimate slightly the stability of the slope, giving an error of -0.09% —point P in Figure 8b. For both Cases 1 and 2, the error is relatively small.

Cases 1 and 2 have also been solved with the *shear strength reduction technique* using the finite different software FLAC (Itasca, Inc. 2016). Figure 9 shows the mesh of elements used for the models. The mesh shown in Figure 9 corresponds to Case 1, for which the elements below the indicated 'firm foundation level' were considered to be elastic.

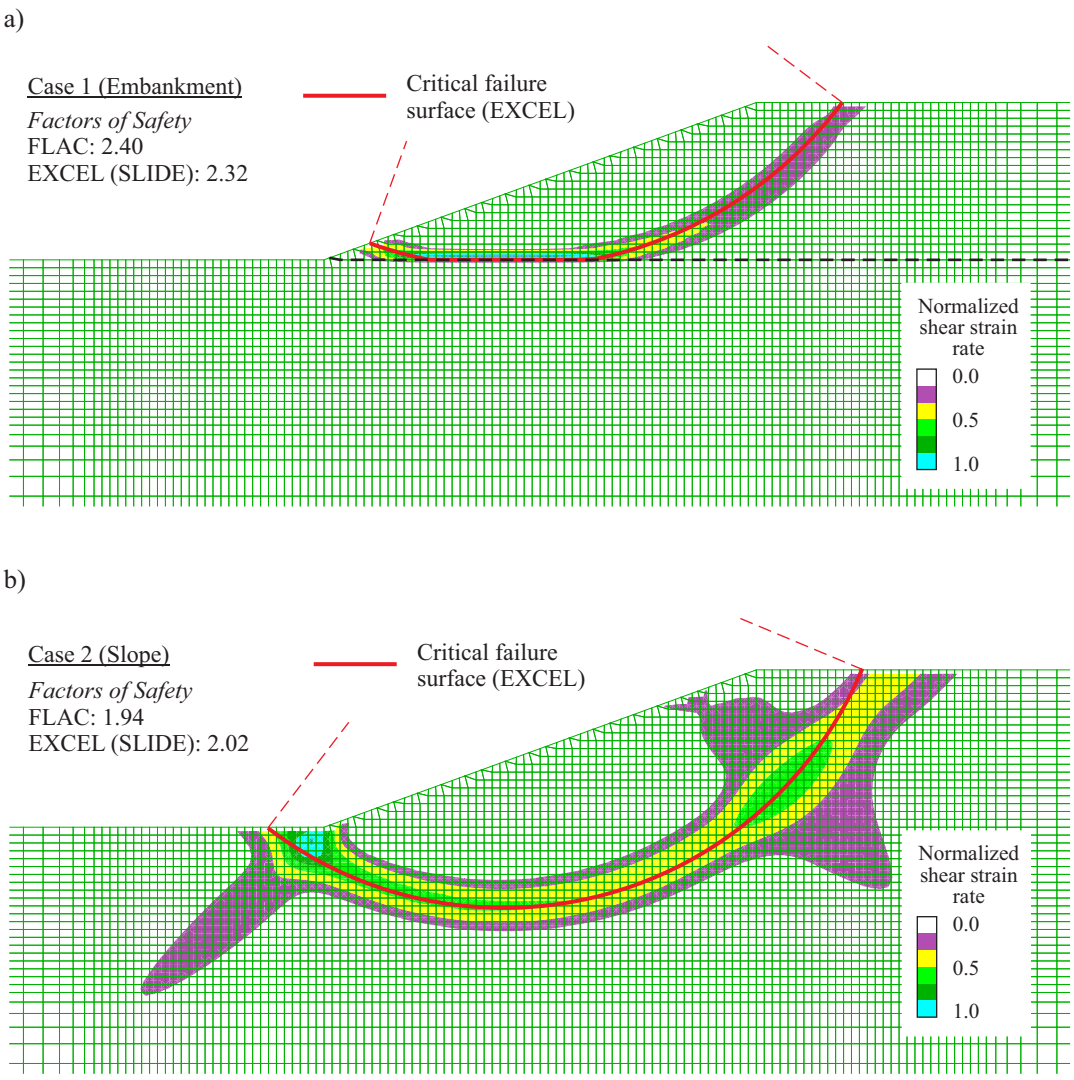

Figure 10. Critical failure surfaces outlined by contours of shear strain rates given by the software FLAC, and as explicitly defined by the EXCEL workbook. Plots correspond to a) Case 1 (*embankment* with firm foundation at the base) and b) Case 2 (*slope*, with firm foundation at great depth).

Figures 10a and 10b show the resulting contours of normalized shear strain computed with the shear strength reduction technique for the models of Case 1 and 2, respectively (these models correspond to models that are at the verge of failure). When applying the shear strength reduction technique, the contour representation of shear strain is normally used to define the critical failure surface. The words 'shear strain' in the legend of Figures 10a and 10b refer to the square root of the second invariant of the deviatoric strain rate, while the word 'normalized' refers to the fact that the shear strain rates have been divided by the maximum value of shear strain rate in the model at the shown state.

Figures 10a and 10b also include the outlines of the critical failure surfaces obtained with the EXCEL workbook —i.e., as obtained with the software SLIDE (Rocscience Inc. 2015). The similarity of the critical failure surfaces obtained with shear strength reduction technique and with the limit equilibrium method is remarkable. In particular, for Case 1 (the embankment case), and according to Steward et al. (2010), the failure surface given by FLAC is *secant* to the firm foundation and not *tangent* as it has been traditionally considered in the literature (Taylor 1948; Bishop & Morgenstern 1960; Morgenstern 1963; Michalowski 2002).

The values of factor of safety obtained with the *shear strength reduction technique* in the software FLAC, and with the *limit equilibrium* method in the EXCEL workbook are indicated on the left side of Figures 10a and 10b. The shear strength reduction technique yields a factor of safety that is comparatively larger than the one obtained with limit equilibrium for Case 1 (Figure 10a), while the opposite is true for the Case 2 (Figure 10b). If the *true* values of factors of safety for the embankment and slope cases are assumed to be the mean values of factors of safety obtained with FLAC and EXCEL (a reasonable assumption considering that there is no *exact* solution for the problem of determining factors of safety), then the normalized errors of the factors of safety for each method result as follows:

For Case 1 (or *embankment* case):

– FLAC, $(2.40-(2.40+2.32)/2)/((2.40+2.32)/2) = 1.69\%$
– EXCEL (SLIDE), $(2.32-(2.40+2.32)/2)/((2.40+2.32)/2) = -1.69\%$

For Case 2 (or *slope* case):

– FLAC, $(1.94-(1.94+2.02)/2)/((1.94+2.02)/2) = -2.02\%$
– EXCEL (SLIDE), $(2.02-(1.94+2.02)/2)/((1.94+2.02)/2) = 2.02\%$

The values listed above indicate that the normalized errors are within approximately $\pm 2\%$ for both Cases 1 and 2, a relative small value that confirms that values of factor of safety obtained with limit equilibrium method and shear strength reduction technique can be expected to be similar for the case of simple embankments and slope cases (Cheng et al. 2007).

Further to the FLAC models discussed above, the results represented in Figure 10 correspond to models with a non-associated flow rule with no dilation. For the particular properties in this application example, the very same factors of safety and contours of shear strain, as represented in Figure 10, were obtained when considering an associated flow rule with a dilation angle equal to the friction angle.

FINAL COMMENTS

The computational tools presented in this paper include graphical dimensionless representations, an EXCEL workbook and regression equations that can be used to quickly determine factors of safety and location of critical circular failure surfaces for simple embankments or slopes in dry homogeneous and isotropic soils. Although these tools were developed for teaching basic slope stability analysis in an undergraduate soil mechanics course, the tools could be useful in geotechnical design practice, for example in the pre-design stage of simple embankments or slopes. The

tools could also be useful when performing probability and reliability analyses of stability of embankments and slopes using the Monte-Carlo simulation technique. In such cases, thousands of cases need to be analyzed to estimate factors of safety for different input parameters (e.g., Vanmarcke 1980; Juang et al. 1998; Wang et al. 2013; Lacasse et al. 2019) and computational tools that allow quick estimation of factors of safety are desirable.

The computational tools presented in this paper will not be applicable to cases of embankments or slopes in *purely cohesive* soil. Indeed, if the internal friction angle of the soil is equal to zero, the dimensionless parameter X in equation (2) becomes undetermined. For the case of embankments or slopes in purely cohesive soil, a new set of tools would be required, with particular consideration that the position of the firm foundation dictates the extent in depth of the critical failure surface. For example, the case of a firm foundation located at infinite depth will always yield an infinitely deep failure surface when the soil is purely cohesive (e.g., Michalowski 2002; Baker 2003; Steward et al. 2010).

The adoption of the *limit equilibrium* method and the Bishop formulation used to develop the tools presented in this paper was due to practical reasons only. Use of commercial limit equilibrium software is still very much spread in the field of geotechnical engineering and the authors needed to generate and solve thousands of models and process the results in a reasonable amount of time. Similar representations could have been developed with *limit analysis* and possibly *shear strength reduction* methods —although in the latter case, an impractical amount of time would have been required to process all models needed to develop these tools. For simple embankment and slope cases considered in this paper (i.e., embankments and slopes with a planar face in homogeneous, isotropic, frictional-cohesive soil) no significant differences in values of factor of safety or location of the critical failure surface could be expected when applying other methods, like limit analysis or shear strength reduction methods (e.g., Yu et al. 1998; Dawnson et al. 1999; Davis & Selvadurai 2005; Cheng et al. 2007; Leshchinsky 2013). Due to the non-existence of a rigorous closed-form solution for the problem of computing the factor of safety and location of the critical failure surface for embankments and slopes, all of the methods available to carry out stability analyses will be expected to give an *approximate* solution to the problem only, and small differences in results of factor of safety and location of the critical failure surface should be always expected, as illustrated in the section 'Application Example' in this paper.

ACKNOWLEDGEMENT

The authors wish to dedicate this paper to their geotechnical engineering professors at the University of Minnesota, Twin Cities Campus, and at University of Michigan, Ann Arbor, respectively. The authors acknowledge that they would not have decided to start a university career to teach geotechnical engineering to young civil engineering students, without the motivation and inspiration received from all outstanding geotechnical engineering professors at the mentioned institutions.

REFERENCES

Abramson, L. W., Lee, T. S., Sharma, S., M., G. & Boyce (2002). *Slope stability and stabilization methods* (2nd ed.). John Wiley & Sons. New York.

Baker, R. (2003). A second look at Taylor's stability chart. *Journal of Geotechnical and Geoenvironmental Engineering 129*(12), 1102–1108.

Bell, J. M. (1966). Dimensionless parameters for homogeneous earth slopes. *Journal of Soil Mechanics & Foundations Div. ASCE SM 5*(GT9), 51–65.

Bishop, A. W. (1955). The use of the slip circle in the stability analysis of slopes. *Géotechnique 5*(1), 7–17.

Bishop, A. W. & Morgenstern, N. R. (1960). Stability coefficients for earth slopes. *Géotechnique 10*(1), 129–150.

Carranza-Torres, C. & Hormazabal, E. (2018). Computational tools for the determination of factor of safety and location of the critical failure surface for slopes in Mohr-Coulomb dry ground. In *Proceedings of the International Symposium Slope Stability 2018. April 11-13, 2018*, Sevilla. Spain. (Available for downoading at www.d.umn.edu/∼carranza/SLOPE18).

Chapra, S. C. & Canale, R. P. (2015). *Numerical methods for engineers* (7th ed.). Mc Graw Hill. New York.

Cheng, Y. M., Lansivaara, T. & Wei, W. B. (2007). Two-dimensional slope stability analysis by limit equilibrium and strength reduction methods. *Computers and Geotechnics 34*(3), 137–150.

Coduto, D. P., Yeung, M. C. & Kitch, W. A. (2011). *Geotechnical engineering. Principles and practices* (2nd ed.). Pearson.

Cousins, B. F. (1978). Stability charts for simple earth slopes. *Journal of the Geotechnical Engineering Division 104*(2), 267–279.

Das, B. M. & Sobhan, K. (2018). *Principles of Geotechnical Engineering* (9th ed.). Cengage.

Davis, R. O. & Selvadurai, A. P. (2005). *Plasticity and geomechanics*. Cambridge University Press.

Dawnson, E. M., Roth, W. H. & Drescher, A. (1999). Slope stability analysis by strength reduction. *Geotechnique 49*(6), 835–840.

Duncan, J. M. (1996). State of the art: limit equilibrium and finite-element analysis of slopes. *Journal of Geotechnical Engineering 122*(7), 577–596.

Duncan, J. M., Wright, S. G. & Brandon, T. L. (2014). *Soil Strength and slope stability*. John Wiley & Sons.

Fine Inc. (2016). *GEO5. Slope stability analysis software based on the limit equilibrium method*. Praha, Czech Republic.

Geo-Slope Inc. (2012). *SLOPE/W Version 2012. Slope stability analysis software based on the limit equilibrium method*. Calgary, Canada.

Griffiths, D. V. & Lane, P. A. (1999). Slope stability analysis by finite elements. *Geotechnique 49*(3), 387–403.

Hammah, R. E., Yacoub, T. E. & Curran, J. H. (2007). Serviceability-based slope factor of safety using the shear strength reduction (SSR) method. In L. R. e Sousa, C. Olalla, & N. Gross-

mann (Eds.), *Proceedings of the 11th Congress of the International Society for Rock Mechanics*, Lisbon.

Hoek, E. (2000). Personal communication.

Hoek, E. & Bray, J. (1974, 1977, 1981). *Rock slope engineering*. Institution of Mining and Metallurgy. London. (First, second and third editions, respectively).

Huang, Y. H. (2014). *Slope stability analysis by the limit equilibrium method. Fundamentals and methods*. American Society of Civil Engineers (ASCE) Press. Reston, Virginia.

Interactive Software Designs Inc. (2007). *XSTABL. Slope stability analysis software based on the limit equilibrium method*. Moscow, Idaho.

Itasca, Inc. (2016). *FLAC (Fast Lagrangian Analysis of Continua) Version 8.0*. Minneapolis, Minnesota: Itasca Consulting Group, Inc.

Janbu, N. (1954)a. Application of composite slip surfaces for stability analysis. In *European Conference on Stability of Earth Slopes.* Stockholm, Sweden, Volume 3, pp. 43–49.

Janbu, N. (1954)b. *Stability analysis of slopes with dimensionless parameters*. Thesis for the Doctor of Science in the Field of Civil Engineering. Harvard University, Soil Mechanics Series, No. 46.

Juang, C. H., Jhi, Y. Y. & Lee, D. H. (1998). Stability analysis of existing slopes considering uncertainty. *Engineering Geology 49*(2), 111–122.

Lacasse, S., Nadim, F., Liu, Z. Q., Eidsvig, U. K., Le, T. M. H. & Lin, C. G. (2019). Risk assessment and dams. Recent developments and applications. In *Proceedings of the XVII European Conference on Soil Mechanics and Geotechnical Engineering (ECSMGE-2019). Geotechnical Engineering foundation of the future.* Reykjavik, Iceland. September 2019.

Leshchinsky, B. (2013). Comparison of limit equilibrium and limit analysis for complex slopes. In *Geo-Congress 2013: Stability and Performance of Slopes and Embankments III*, pp. 1280–1289.

Mesri, G. & Shahien, M. (2003). Residual shear strength mobilized in first-time slope failures. *Journal of Geotechnical and Geoenvironmental Engineering 129*(1), 12–31.

Michalowski, R. L. (2002). Stability charts for uniform slopes. *Journal of Geotechnical and Geoenvironmental Engineering. ASCE 128-4*(GT9), 351–355.

Michalowski, R. L. (2013). Stability assessment of slopes with cracks using limit analysis. *Canadian Geotechnical Journal 50*, 1011–1021.

Microsoft (2016). *Excel Software. Version 2016*. Microsoft. Redmond, Washington.

Morgenstern, N. R. (1963). Stability charts for earth slopes during rapid drawdown. *Géotechnique 13*(1), 121–131.

Morgenstern, N. R. & Price, V. E. (1965). The analysis of the stability of general slip surfaces. *Géotechnique 15*(1), 77–93.

Mostyn, G. R. & Small, J. C. (1987). Methods of stability analysis. In B. F. Walker & R. Fell (Eds.), *Soil slope stability*, pp. 71–120. Balkema. Rotterdam.

O'Connor, M. J. & Mitchell, R. J. (1977). An extension of the Bishop and Morgenstern slope stability charts. *Canadian Geotechnical Journal 14*(1), 144–151.

Potts, D. M. & Zdravkovic, L. (1999). *Finite element analysis in geotechnical engineering. Theory*.

Thomas Telford. London: Thomas Telford.

Rocscience Inc. (2015). *SLIDE Version 7. Slope stability analysis software based on the limit equilibrium method*. Toronto, Canada.

Scott, C. R. (1994). *An Introduction to Soil Mechanics and Foundations* (3rd ed.). Springer-Science & Business Media, B.V.

Spencer, E. (1967). A method of analysis of the stability of embankments assuming parallel inter-slice forces. *Géotechnique 17*, 11–26.

Spencer, E. (1973). Thrust line criterion in embankment stability analysis. *Géotechnique 23*, 85–100.

Steward, T., Sivakugan, N., Shukla, S. K. & Das, B. M. (2010). Taylor's slope stability charts revisited. *International Journal of Geomechanics 11*(4), 348–352.

Taylor, D. W. (1948). *Fundamentals of Soil Mechanics*. Wiley. New York.

Terzaghi, K., Peck, R. B. & Mesri, G. (1996). *Soil mechanics in engineering practice*. John Wiley & Sons.

Utili, S. (2013). Investigation by limit analysis on the stability of slopes with cracks. *Geotechnique 6*(2), 140–154.

Utili, S. & Abd, A. H. (2016). On the stability of fissured slopes subject to seismic action. *International Journal for Numerical and Analytical Methods in Geomechanics 40*, 785–806.

Vanmarcke, E. H. (1980). Probabilistic stability analysis of earth slopes. *Engineering Geology 16*(1-2), 29–50.

Verruijt, A. (2012). *Soil Mechanics*. Delft University of Technology, Delft, The Netherlands (Available for dowloading at http://geo.verruijt.net/).

Wang, L., Hwang, J., Juang, H. & Atamturktur, S. (2013). Reliability-based design of rock slopes. A new perspective on design robustness. *Engineering Geology 154*, 56–63.

Wyllie, D. C. (2018). *Rock slope engineering. Civil Applications* (5th ed.). CRC Press. Taylor & Francis.

Wyllie, D. C. & Mah, C. (2004). *Rock slope engineering. Civil and Mining* (4th ed.). CRC Press.

Yu, H. S., Salgado, R., Sloan, S. W. & Kim, J. M. (1998). Limit analysis versus limit equilibrium for slope stability. *Journal of Geotechnical and Geoenvironmental Engineering 124*(1), 1–11.